MDPI

Article

Direct Deviations in Astrocyte Free Ca²⁺ Concentration Control Multiple Arteriole Tone States

Jordan N. Haidey and Grant R. Gordon *

Hotchkiss Brain Institute, Department of Physiology and Pharmacology, Cumming School of Medicine, University of Calgary, Calgary, AB T2N 4N1, Canada; jnhaidey@ucalgary.ca
* Correspondence: gordong@ucalgary.ca

Abstract: Astrocytes elicit bidirectional control of microvascular diameter in acutely isolated brain slices through vasoconstriction and vasodilation pathways that can be differentially recruited via the free Ca^{2+} concentration in endfeet and/or the metabolic status of the tissue. However, the Ca^{2+}-level hypothesis has not been tested using direct manipulation. To overcome this, we used Ca^{2+}-clamp whole-cell patching of peri-arteriole astrocytes to change astrocyte-free Ca^{2+} to different concentrations and examined the vascular response. We discovered that clamping Ca^{2+} at the approximate resting value (100 nM) had no impact on arteriole diameter in a pre-constricted arteriole. However, a moderate elevation to 250 nM elicited sustained vasodilation that was blocked by the COX-1 antagonist SC-560 (500 nM). The vasodilation to 250 nM Ca^{2+} was sensitive to the metabolic state, as it converted to vasoconstriction when oxygen tension was dramatically elevated. In normal oxygen, clamping astrocyte Ca^{2+} well above the resting level (750 nM) produced sustained vasoconstriction, which converted to vasodilation in the 20-HETE blocker HET0016 (1 μM). This response was fully blocked by the addition of SC-560 (500 nM), showing that 20-HETE-induced vasoconstriction dominated the dilatory action of COX-1. These data demonstrate that direct changes in astrocyte free Ca^{2+} can control multiple arteriole tone states through different mediators.

Keywords: astrocyte; calcium; two-photon; patch clamp; arteriole; tone; steady-state

1. Introduction

Ca^{2+}-dependent signaling in astrocytic endfeet contributes to the regulation of arteriole diameter [1–3]. While different transmitters and G-protein-coupled receptors drive distinct cell pathways that cause different vascular responses, it is notable that within the neurovascular unit, even the same transmitter and receptor system can elicit vasoconstriction or vasodilation depending on the physiological context or the current state of the microenvironment. These include the level of free Ca^{2+} in astrocyte endfeet [4], the degree of arteriole tone [5,6], and the metabolic status of the tissue [7,8]. These different scenarios may not be completely mechanistically separate, as both increases in arteriole tone and low oxygen levels elevate astrocyte free Ca^{2+} [6,9,10]. In acute brain slices, when using afferent stimulation or direct Ca^{2+} uncaging in astrocytes, a small elevation in free Ca^{2+} above baseline yielded vasodilation of penetrating arterioles in the neocortex, whereas a larger elevation in free Ca^{2+} caused vasoconstriction [4]. A similar concept was proposed to explain differential vessel responses to seizure activity in a 4-AP model of epilepsy in vivo [11] and the observation of vasoconstriction during spreading depression in vivo where the intracellular Ca^{2+} level became high [12]. The $[Ca^{2+}]_i$ crossover point to see these different responses was determined to be ~500 nM in astrocytes by calculating the concentration based on the observed $\Delta F/F$ and by determining the max $\Delta F/F$ at the end of each experiment with a Ca^{2+} ionophore [4]. An alternative method for testing this hypothesis is to directly 'clamp' astrocyte free Ca^{2+} at different concentrations via a patch pipette, though this method has not yet been performed to either support or refute the hypothesis.

Direct Ca^{2+} clamping of astrocytes also allows one to explore how sustained changes in astrocyte-free Ca^{2+} impact vascular tone. For example, it is unclear if arteriole diameter tracks long-lasting changes in astrocyte Ca^{2+} or if any evoked vascular response is transient in nature. This is important because most investigations have focused on brief vascular responses to astrocyte Ca^{2+} transients. However, astrocytes have been more recently implicated in the regulation of ongoing arteriole tone, independent of neural activity. This may occur through the steady-state Ca^{2+} concentration in astrocyte/Müller cell endfeet [13,14], relatively small elevations in endfoot Ca^{2+} evoked by static or rhythmic arteriole constrictions [6], and/or elevations in endfoot Ca^{2+} in response to increases in intraluminal pressure [9]. Similar tonic effects on astrocyte Ca^{2+} and arteriole diameter have also been observed after plasticity-inducing trains of afferent stimulation in neocortical slices [15]. Nevertheless, it remains unclear how directly maintaining astrocyte free Ca^{2+} at specific concentrations affects the arteriole response. We tested the hypothesis that arteriole tone tracks sustained changes to astrocyte free Ca^{2+} in a bidirectional manner depending on the absolute Ca^{2+} concentration.

2. Materials and Methods

All procedures abided by Canadian standards for animal research and were approved by the Animal Care and Use Committee of the University of Calgary (protocol AC19-0109). Male Sprague Dawley rats (P23-30, Charles River, Wilmington, MA, USA) received an intravenous injection of fluorescein isothiocyanate–dextran (FITC–dextran) (Sigma-Aldrich, St. Louis, MO, USA, 2000 KDa; 15 mg in 0.4 mL lactated ringers) to visualize the vasculature. Acute coronal slices of the sensory–motor cortex were cut with a vibratome (Leica VT1200S) while submerged in a slicing solution containing (in mM): N-methyl d-glucamine (119.9), KCl (2.5), $NaHCO_3$ (25), $CaCl_2$–$2H_2O$ (1.0), $MgCl_2$–$6H_2O$ (6.9), NaH_2PO_4–H_2O (1.4), and glucose (20). Brain slices then recovered in artificial cerebrospinal fluid (ACSF) continuously bubbled with carbogen (95% O_2 and 5% CO_2) at 34 °C for 45 min. ACSF contained (in mM): NaCl (126), KCl (2.5), $NaHCO_3$ (25), $CaCl_2$ (1.5), $MgCl_2$ (1.2), NaH_2PO_4 (1.25), and glucose (10). Slices were bulk-loaded with Rhod-2/AM (Biotium Inc.) at 15 µM (0.2% DMSO; 0.006% pluronic acid; 0.0002% Cremophor EL (Sigma-Aldrich)) for 45 min in carbogen-bubbled ACSF. Slices were transferred to ACSF continuously bubbled with physiological levels of oxygen (30%) and were provided 45 min to equilibrate. In a subset of experiments, slices were maintained in a high oxygen condition (carbogen). The arteriole pre-constrictor U-46619 (Cayman Chemical, Ann Arbor, MI, USA) (100 nM) was added to the bath for all experiments. Fluorescence imaging was performed with a custom two-photon laser-scanning microscope [16] equipped with a 40x W/1.0 NA Zeiss objective lens and a Chameleon Ultra Ti:Sapph laser (Coherent, Santa Clara, CA, USA). Imaging was performed at 22 °C, and slices were superfused with ACSF (aerated with 30% or 95% O_2) at ~2 mL/min.

Astrocytes were identified by bright Rhod2/AM uptake, endfeet opposing the vasculature, and input resistance (10–20 mΩ). Astrocytes that were ~30–60 microns from the coronal surface of the slice and less than ~60 microns from a penetrating arteriole were targeted for patch clamp. A giga-ohm seal was maintained for ~10–20 min prior to imaging to allow the effects of the patching process on arteriole tone and Ca^{2+} signal to subside. We recorded 100 s of stable baseline prior to going whole-cell and allowing the internal solution (visualized by Alexa 488; 200 µM) to diffuse throughout the astrocyte network. Astrocyte Ca^{2+} was clamped at different target concentrations by patching with internal solutions containing different ratios of BAPTA and free Ca^{2+}. The base internal solution contained (in mM): potassium gluconate (68), KCl (8), sodium gluconate (8), $MgCl_2$ (2), HEPES (10), potassium ATP (4), sodium GTP (0.3), and potassium BAPTA (10). To clamp astrocyte Ca^{2+} at different concentrations, the $CaCl_2$ concentration was adjusted in each internal solution. The 100, 250, and 750 nM Ca^{2+} clamp solutions contained 0.043, 0.067, and 0.086 mM $CaCl_2$, respectively, as derived with the Maxchelator Calculator [17]. Once in whole-cell configuration, astrocytes were voltage clamped at -80 mV. A stable holding current and input resistance were monitored throughout the experiment, and the rate and

extent of Alexa-488 filling in endfeet were quantified to ensure comparable results across groups. ImageJ (National Institutes of Health, Bethesda, MD, USA) and Prism 7 software (GraphPad, La Jolla, CA, USA) were used to analyze the data.

Rhod-2/AM intensity over time was analyzed to measure relative changes in astrocyte endfoot Ca^{2+} signal as $\Delta F/F = ((F_1 - F_0)/F_0) \times 100$. Lumen area was measured to assess changes in arteriole diameter using particle analysis in ImageJ. The baseline Rhod-2/AM signal and arteriole diameter were compared to peak values, the latter of which were determined by examining the average trace data to find the time in which the peak occurred. This time point was then used to extract a measurement from each of the individual experiments for statistical comparison. $p < 0.05$ was deemed statistically significant. Paired student's t-tests were used to assess changes within groups (comparing baseline to peak). Unpaired t-tests were used to compare the 250 nM Ca^{2+} clamp in 30–95% O_2 conditions. A one-way ANOVA was used to compare peak means across groups with Tukey's multiple comparisons.

3. Results

3.1. Clamping Astrocyte Ca^{2+} to Different Elevated Levels Elicits Opposite Arteriole Tone States

Using a whole-cell patch technique designed to buffer free Ca^{2+} to a particular target concentration using BAPTA plus $CaCl_2$ [18], we tested the hypothesis that clamping astrocyte Ca^{2+} near resting physiological levels would have little impact on existing arteriole tone. Quantitative Ca^{2+} imaging studies have reported resting astrocyte Ca^{2+} levels of ~80–130 nM [19–21], so we clamped astrocyte Ca^{2+} at 100 nM. Neocortical brain slices were bulk-loaded with a Rhod-2/AM Ca^{2+} indicator, arterioles were pre-constricted with U-46619 (100 nM), and the tissue was equilibrated in physiological levels of O_2 (30%) before the start of the astrocyte patching experiment. After sealing onto an astrocyte soma, on-cell configuration was maintained for ~15 min before going whole-cell. The time course and extent of internal solution diffusion into the patched astrocyte, its adjoining endfoot, and additional spread throughout the astrocyte network were visualized with Alexa-488 (200 µM) [13]. Following the arrival of the Alexa-488 signal (along with BAPTA-base Ca^{2+}-clamp solution) into astrocyte endfeet, we observed no significant change in arteriole diameter ($2.2 \pm 1.0\%$, $n = 5$, $p > 0.05$; Figure 1A–D). To test whether moderately elevating astrocyte Ca^{2+} produced vasodilation, we patched astrocytes to deliver a BAPTA-containing internal solution designed to clamp intracellular Ca^{2+} at 250 nM, which was above an approximate resting value of 100 nM [21]. In response to this manipulation, we observed a sustained vasodilation ($12.6 \pm 2.7\%$, $n = 8$, $p < 0.01$; Figure 1E,G,H) that lasted the duration of the recording (~8 min). We observed a significant increase in relative endfoot Ca^{2+} signal ($\Delta F/F_{Rhod-2} = 37.0 \pm 15.1\%$, $p < 0.05$; Figure 1F–H), thus confirming that the 250 nM Ca^{2+} solution elevated Ca^{2+} from baseline concentration. We then tested whether the vasodilation evoked by 250 nM free Ca^{2+} in astrocytes was sensitive to the metabolic status of the tissue, as dictated by oxygen availability. Similar to previous reports [7,8], increasing the O_2 to supra-physiological levels (95%) switched the vasodilation to vasoconstriction ($-7.4 \pm 3.0\%$, $n = 7$, $p < 0.01$; Figure 1N,S) despite the same increase in Ca^{2+} within astrocytes ($p = 0.3$; Figure 1Q,S).

Next, to examine the effect of a high increase in endfoot Ca^{2+} on arteriole tone at physiological levels of O_2, we clamped astrocyte Ca^{2+} at 750 nM. The arrival of Alexa-488 to the endfeet corresponded with a long-lasting arteriole constriction ($-8.4 \pm 1.6\%$, $n = 8$, $p < 0.01$; Figure 1I,K,L) and a rapid, sustained increase in relative Ca^{2+} signal ($\Delta F/F_{Rhod-2} = 92.6 \pm 36.3\%$, $p < 0.05$; Figure 1J–L). We measured the tau of the monophasic exponential arrival of the Alexa-488 signal in endfeet to control for differences in the time course of internal solution delivery between experimental conditions [13]. There was no significant difference in tau values between the various Ca^{2+} clamp groups ($p > 0.05$; Figure 1O,R). Consequently, the observed differences in both vascular tone and relative endfoot Ca^{2+} cannot be attributed to the differential kinetics of internal solution diffusion through the astrocyte network.
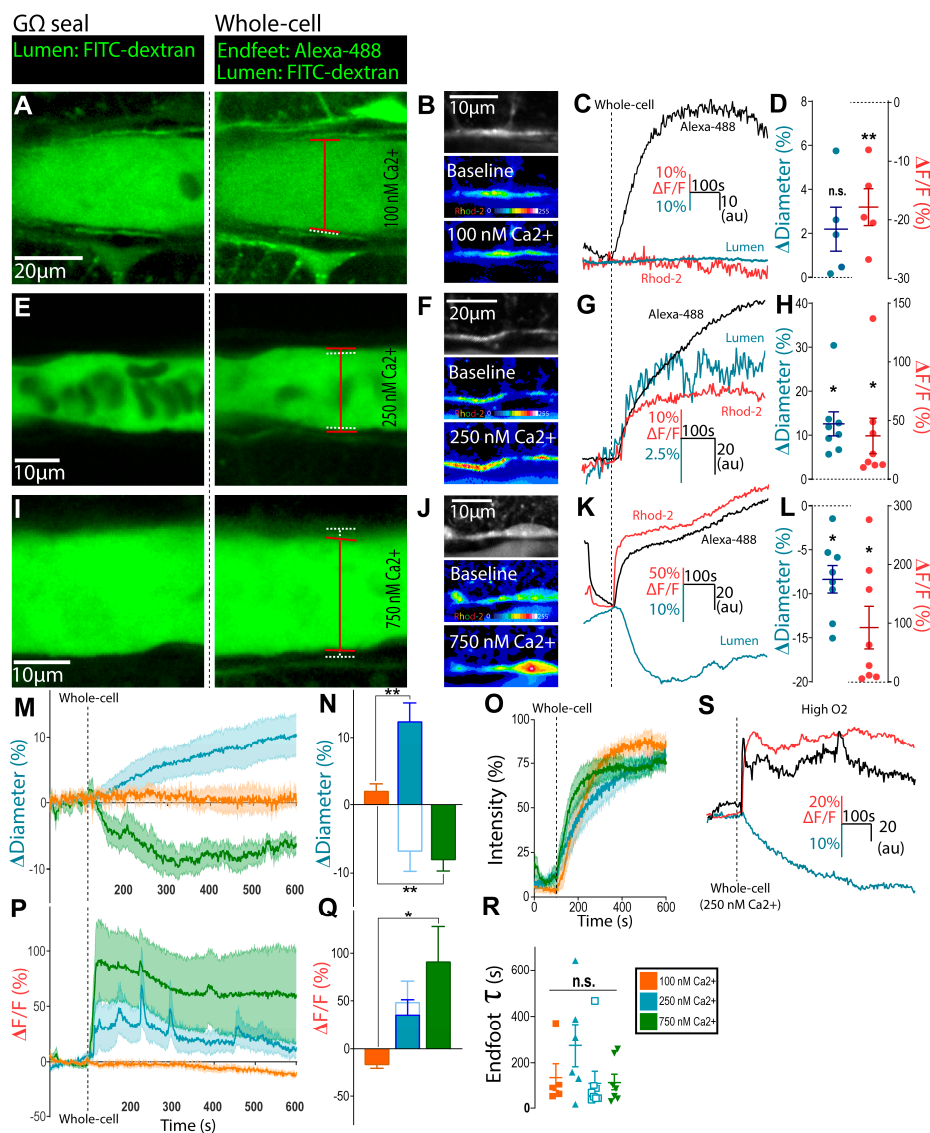
Figure 1. Astrocyte endfoot Ca^{2+} controls multiple arteriole tone states. (**A**) Representative image during astrocyte on-cell ($G\Omega$ seal, left) and whole-cell configuration (right) to clamp endfoot Ca^{2+} at 100 nM in rats; the lumen were visualized with FITC–dextran, and endfoot filling was visualized with Alexa-488. Diameter measurements before (white, dashed) and after (red, solid) are shown. (**B**) Representative images showing endfoot Rhod-2 Ca^{2+} signal in grayscale (top), in on-cell configuration (middle), and after switching to whole-cell configuration to deliver 100 nM Ca^{2+} clamp solution. Rainbow pseudocolor shows relative Rhod-2 fluorescence, with hotter colors corresponding with greater intensity. (**C**) Representative endfoot Alexa-488 (black), diameter (blue), and Rhod-2 Ca^{2+} (red) traces in response to 100 nM Ca^{2+} clamp. (**D**) Summary diameter and Rhod-2 endfoot Ca^{2+} data. Data are mean $\pm$ SEM. (**E–H**) Same as (**A–D**) but for the 250 nM Ca^{2+} clamp. (**I–L**) Same as (**A–D**) but with the 750 nM Ca^{2+} clamp. (**M,P**) Summary time series data of arteriole diameter (**M**) and endfoot Ca^{2+} (**P**) in response to the different Ca^{2+} clamp conditions; data are mean $\pm$ SEM. (**N,Q**) Summary data of changes in arteriole diameter (**N**) and endfoot Ca^{2+} (**Q**) in response to the various Ca^{2+} clamp conditions; data are mean $\pm$ SEM. (**O,R**) Average tau traces (**O**) and summary values (**R**) of the monophasic exponential arrival of Alexa-488 to astrocytic endfeet were not different between the various Ca^{2+} clamp conditions; data are mean $\pm$ SEM. (**S**) Same as (**G**) but in 95% O_2-bubbled superfusate. * $p < 0.05$, ** $p < 0.01$.

3.2. Bidirectional Changes in Arteriole Diameter Evoked by Elevations in Astrocyte Ca^{2+} Are Mediated by COX-1 and 20-HETE

We previously demonstrated that lowering astrocyte Ca^{2+} below the resting level with intracellular BAPTA next to a pre-constricted arteriole induced vasoconstriction. This effect was eliminated by the COX-1 blocker SC-560 and astrocyte Ptgs1 knockdown [6]. This suggested that the resting endfoot Ca^{2+} level (in part determined by arteriole tone itself)

produced the tonic release of vasodilators via COX-1 activity. To determine whether 250 nM Ca^{2+}-clamp-evoked vasodilation was mediated by the further activation of COX-1, we repeated this experiment in the presence of SC-560 (500 nM) (Figure 2A–D). Pre-treatment of brain slices with this COX-1 antagonist blocked 250 nM Ca^{2+} clamp-evoked vasodilation ($-1.3 \pm 1.6\%$, $n = 5$, $p = 0.007$), despite no differences in either the relative Ca^{2+} increase ($p = 0.2$) of the rate of endfoot filling ($p = 0.9$) (Figure 2D).
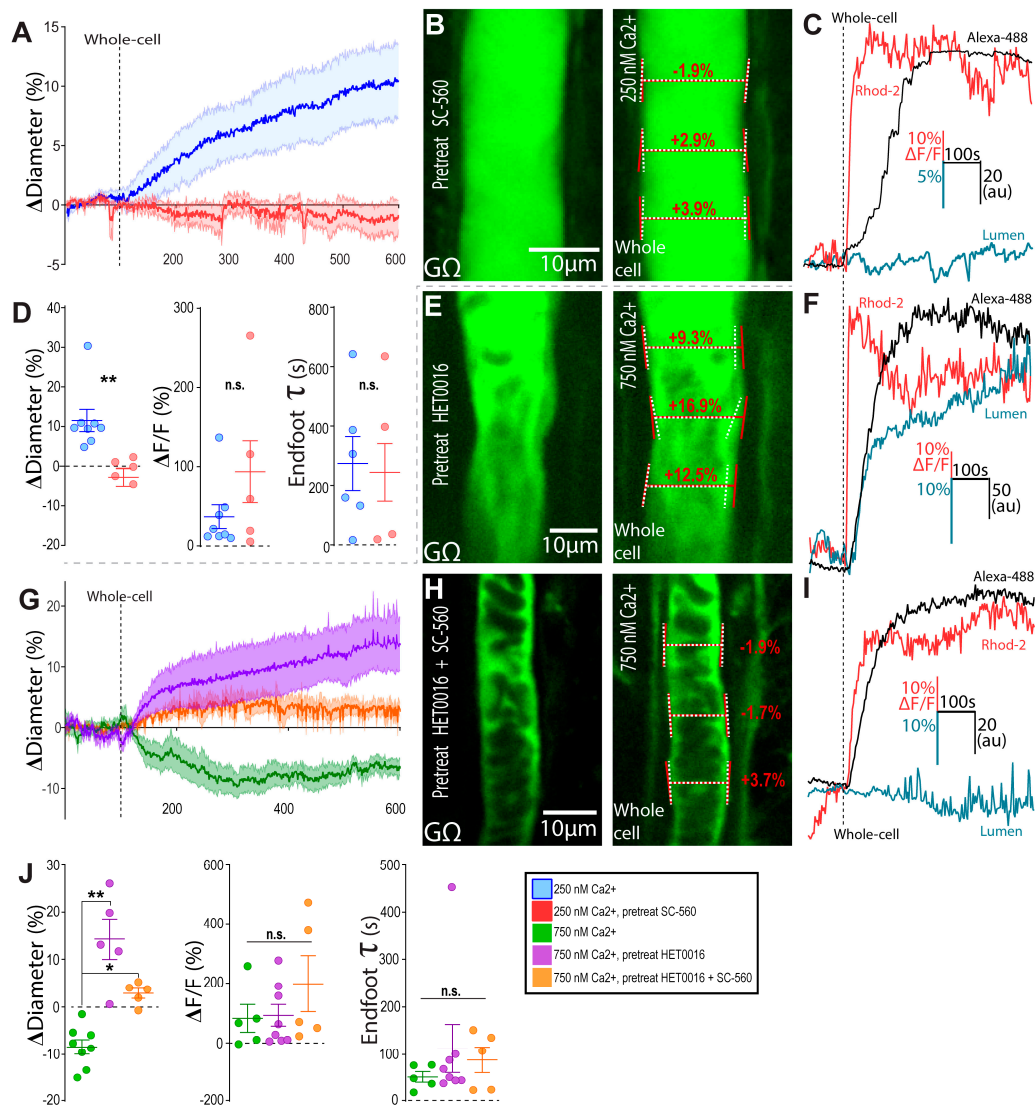
Figure 2. Increases in astrocyte free Ca^{2+} engage COX-1 and 20-HETE. (**A**) Summary time series of arteriole diameter in response to 250 nM Ca^{2+} clamp pretreated with SC-560 (500 nM) (red) versus control (blue). Central bolded lines represent mean values, while the shaded areas represent $\pm$ SEM. (**B**) Representative images during astrocyte on-cell (GΩ seal, left) and whole-cell configuration (right) in response to 250 nM Ca^{2+} clamp pretreated with SC-560 (500 nM). Diameter measurements before (white, dashed) and after (red, solid) are shown. (**C**) Representative endfoot Alexa-488 (black), diameter (blue), and Rhod-2 Ca^{2+} (red) traces in response to 250 nM Ca^{2+} clamp pretreated with SC-560. (**D**) Summary diameter, Rhod-2 endfoot Ca^{2+}, and endfoot Alexa-488 tau data in response to 250 nM Ca^{2+} clamp pretreated with SC-560 (red) and control (blue); data are mean $\pm$ SEM. (**E,F**) Same as (**B,C**) but for the 750 nM Ca^{2+} clamp pretreated with HET0016 (1 μM). (**G**) Summary time series of arteriole diameter in response to the 750 nM Ca^{2+} clamp pretreated with 1 μM HET0016 (purple), 1 μM HET0016 plus 500 nM SC-560 (orange), and control (green). Central bolded lines represent mean values, while the shaded areas represent $\pm$ SEM. (**H,I**) Same as (**B,C**) but for the 750 nM Ca^{2+} clamp pretreated with both SC-560 (500 nM) and HET0016 (1 μM). (**J**) Summary diameter, Rhod-2 endfoot Ca^{2+}, and endfoot Alexa-488 tau data in response to the 750 nM Ca^{2+} clamp pretreated with 1 μM HET0016 (purple), 1 μM HET0016 plus 500 nM SC-560 (orange), and control (green). * $p < 0.05$, ** $p < 0.01$.

High astrocyte Ca^{2+}-induced vasoconstriction has been previously linked to arachidonic acid conversion to the potent vasoconstrictor 20-HETE [2,22], ATP release and P2Y1 receptor activation [23], and BK channel opening with K^+ efflux [4]. Given that our Ca^{2+} clamp approach at 250 nM was generating AA due to COX-1 recruitment, we tested whether 750 nM astrocyte Ca^{2+} resulted in enough AA to drive the 20-HETE constriction pathway to dominate vasodilatory prostaglandins. Indeed, the presence of the CYP450 blocker HET0016 (1 μM), used to block the synthesis of 20-HETE, reversed the vascular response to 750 nM astrocyte Ca^{2+} from a constriction (-8.4 ± 1.6, $n = 8$) to a dilation ($14.3 \pm 4.3\%$, $n = 5$, $p = 0.009$) (Figure 2E–G). To test the idea that this reversal in diameter response in HET0016 was due to an intact vasodilatory COX-1 pathway in high intracellular Ca^{2+}, we pre-treated slices with HET0016 plus SC560. In this cocktail, 750 nM astrocyte Ca^{2+} elicited no significant changes in vascular tone ($2.9 \pm 1.0\%$, $n = 5$, $p < 0.0001$) (Figure 2G–J).

4. Discussion

Here, we found that two different and direct elevations from the resting astrocyte Ca^{2+} concentration controlled opposite arteriole tone states, whereas clamping astrocyte Ca^{2+} at the presumed resting level caused no change in diameter. Specifically, we observed that clamping astrocyte Ca^{2+} at a moderate level above resting (250 nM) elicited vasodilation that was eliminated by the COX-1 antagonist SC-560 (500 nM). A high Ca^{2+} concentration (750 nM) produced arteriole constriction that was reversed to dilation by the 20-HETE blocker HET0016 (1 μM) and fully eliminated by a cocktail of SC-560 (500 nM) and HET0016 (1 μM). Though previous investigations have predominantly examined vascular responses to astrocyte Ca^{2+} transients, our data showed that arteriole tone tracks sustained changes to astrocyte free Ca^{2+}.

A previous study using calculation-based $[Ca^{2+}]_i$ estimation in astrocytes placed the crossover point for astrocytes evoking vasodilation to vasoconstriction at ~500 nM [4]. This corresponds well with our data, in which clear opposite arteriole responses were observed when the Ca^{2+} concentration straddled this value at 250 and 750 nM using patch pipettes to directly control free Ca^{2+}. The previous work describing opposing arteriole responses to elevations of free Ca^{2+} to different levels provided mechanistic data in support of BK channels in endfeet [4]. While our work supports AA metabolites in these patch-evoked effects, BK channels were not explored, though they may have contributed to our described effects via the PGE2-mediated opening of BK channels [24]. Alternatively, prostaglandin release and K^+ efflux from endfeet may cooperatively act on vascular smooth muscle membrane potential.

This vascular polarity-switching phenomenon occurs in other conditions. Previously, the metabolic state of brain tissue determined the polarity of vascular responses to Ca^{2+} uncaging events in astrocytes [7] or neural activity [8]. Consistent with this, we found that clamping astrocyte Ca^{2+} at 250 nM elicited arteriole dilation in 30% O_2 and vasoconstriction was produced in supra-physiological O_2 (95%). The effector molecules released by physiological levels of O_2 may be lactate and adenosine, which help promote vasodilation and block vasoconstriction, respectively [7]. Additionally, large differences in arteriole tone induced by U-46619 permit opposite arteriole responses to the same mGluR agonist, t-ACPD [5]. When strongly constricted, t-ACPD produces vasodilation, and when the vessel is much more relaxed, t-ACPD generates vasoconstriction. However, in our study, we used a consistent and constant degree of tone (~20%) elicited by U-46619 (100 nM) across experiments; thus, differences in tone were unlikely to be a major factor, though this may have contributed to within-group variability.

Our data provide support for the idea that 20-HETE-mediated vasoconstriction dominates prostaglandin-mediated vasodilation pathways. Similar trends, in which constriction overpowers active dilation pathways were reported for oxygen and for K^+. For O_2, astrocyte-mediated vasoconstriction dominated dilation in the high O_2 condition unless adenosine and lactate were provided to the extracellular milieu [7]. For K^+, ongoing K^+-mediated dilation can be overcome by vasoconstriction when a certain threshold con-

centration of K^+ was reached [4]. Such a switch to an entirely different vessel response is readily explained by the sudden opening of L-type Ca^{2+} channels in vascular smooth muscle as threshold membrane potential is reached, either through the action of different mediators (PGE2 vs. 20-HETE) or when external K^+ becomes high enough to drive intracellular depolarization rather than hyperpolarization [1,2,25–27].

An important limitation of our work was the use of acute brain slices, maintained at room temperature and containing arterioles that lack blood flow and perfusion pressure. Though an unrealistic preparation, our data, which show vasodilation at modest levels of astrocyte free Ca^{2+} and vasoconstriction at higher levels, are consistent with in vivo studies [11,12,25], one of which employed quantitative Ca^{2+} measurements with fluorescence lifetime imaging microscopy (FLIM) [11]. Another limitation was our inability to confirm the $[Ca^{2+}]_i$-clamp achieved in endfeet. Though we directly patched astrocytes abutting arterioles, both the concentration of BAPTA and free Ca^{2+} in the Ca^{2+}-clamp solution was somewhat lower in the endfeet compared to the patch pipette and significantly lower in neighboring astrocytes as measured by FLIM [21]. Assuming equal reductions in both [BAPTA] and $[Ca^{2+}]$ as distance increases from the pipette within the patched astrocyte, the clamp should still occur at the same intended Ca^{2+} concentration but the overall buffering capacity of the solution will be less (i.e., less able to deal with increases or decreases away from this equilibrium). Future work could employ quantitative Ca^{2+} measurements to understand the exact changes, but the opposite vascular responses we measured under our different patch conditions indicated clear differences in the achieved Ca^{2+} concentrations.

The role of astrocytes in brief, stimulus-evoked, functional hyperemia is debated [28–35]. However, astrocytes express COX-1 [36,37] and downstream microsomal prostaglandin synthase [38], and this pathway may contribute to the regulation of arteriole diameter [39,40]. However, several groups have reported no role of COX-1 in functional hyperemia [36,41,42]. Clarifying this, recent work demonstrated that at least one role of COX-1 in astrocytes is to help constrain the degree vasoconstriction through an arteriole–endfoot feedback mechanism [6]. In vivo, astrocytic *Ptgs1* knockdown experiments revealed that COX-1 helped constrain the power of rhythmic oscillations in arteriole diameter over a wide range of very low frequencies [6]. Additional or complementary roles for astrocytic-COX-1 could include mediating CO_2-induced vasodilation [38] or mediating capillary dilation to afferent neural activity [37]. At this point, it remains unclear which of these roles is relevant for our 250 nM Ca^{2+}-recruitment of COX-1. The recruitment of 20-HETE at high levels of Ca^{2+} may be important for neuromodulators such as noradrenaline that evoke large Ca^{2+} elevations in astrocytes and vasoconstriction through this pathway [2] or during pathological events such as spreading depression when astrocyte Ca^{2+} is aberrantly elevated [43,44]. Nevertheless, we have demonstrated that these pathways can be constantly engaged in a steady-state manner depending on the set concentration of astrocyte Ca^{2+}. Additionally, our data further support the idea that the level of endfoot Ca^{2+} helps dictate the polarity of the arteriole response, that such responses are sensitive to the metabolic micro-environment, and that constrictions readily dominate active dilation pathways.

Author Contributions: Conceptualization, J.N.H. and G.R.G.; methodology, J.N.H. and G.R.G.; formal analysis, J.N.H.; investigation, J.N.H.; data curation, J.N.H.; writing—original draft preparation, J.N.H.; writing—review and editing, J.N.H. and G.R.G.; supervision, G.R.G.; funding acquisition, G.R.G. All authors have read and agreed to the published version of the manuscript.

Institutional Review Board Statement: The study was conducted according to the guidelines set forth by the Canadian Council on Animal Care, and approved by the Animal Ethics Committee of the University of Calgary (protocol AC19-0109).

Informed Consent Statement: Not applicable.

References

1. Zonta, M.; Angulo, M.C.; Gobbo, S.; Rosengarten, B.; Hossmann, K.-A.; Pozzan, T.; Carmignoto, G. Neuron-to-astrocyte signaling is central to the dynamic control of brain microcirculation. *Nat. Neurosci.* **2003**, *6*, 43–50. [CrossRef]

2. Mulligan, S.J.; MacVicar, B.A. Calcium transients in astrocyte endfeet cause cerebrovascular constrictions. *Nature* **2004**, *431*, 195–199. [CrossRef] [PubMed]

3. Filosa, J.A.; Bonev, A.D.; Nelson, M.T. Calcium Dynamics in Cortical Astrocytes and Arterioles during Neurovascular Coupling. *Circ. Res.* **2004**, *95*, e73–e81. [CrossRef] [PubMed]

4. Girouard, H.; Bonev, A.D.; Hannah, R.M.; Meredith, A.; Aldrich, R.W.; Nelson, M.T. Astrocytic endfoot Ca2+ and BK channels determine both arteriolar dilation and constriction. *Proc. Natl. Acad. Sci. USA* **2010**, *107*, 3811–3816. [CrossRef] [PubMed]

5. Blanco, V.M.; Stern, J.E.; Filosa, J.A. Tone-dependent vascular responses to astrocyte-derived signals. *Am. J. Physiol.-Heart Circ. Physiol.* **2008**, *294*, H2855–H2863. [CrossRef] [PubMed]

6. Haidey, J.N.; Peringod, G.; Institoris, A.; Gorzo, K.A.; Nicola, W.; Vandal, M.; Ito, K.; Liu, S.; Fielding, C.; Visser, F.; et al. Astrocytes regulate ultra-slow arteriole oscillations via stretch-mediated TRPV4-COX-1 feedback. *Cell Rep.* **2021**, *36*, 109405. [CrossRef]

7. Gordon, G.; Choi, H.; Ellis-Davies, G.; MacVicar, B. Brain metabolic state dictates the polarity of astrocyte control over the cerebrovasculature. *Nature* **2008**, *456*, 745–749. [CrossRef]

8. Mishra, A.; Hamid, A.; Newman, E.A. Oxygen modulation of neurovascular coupling in the retina. *Proc. Natl. Acad. Sci. USA* **2011**, *108*, 17827–17831. [CrossRef]

9. Kim, K.J.; Iddings, J.A.; Stern, J.E.; Blanco, V.M.; Croom, D.; Kirov, S.A.; Filosa, J.A. Astrocyte Contributions to Flow/Pressure-Evoked Parenchymal Arteriole Vasoconstriction. *J. Neurosci.* **2015**, *35*, 8245–8257. [CrossRef]

10. Angelova, P.R.; Kasymov, V.; Christie, I.; Sheikhbahaei, S.; Turovsky, E.; Marina, N.; Korsak, A.; Zwicker, J.; Teschemacher, A.G.; Ackland, G.L.; et al. Functional Oxygen Sensitivity of Astrocytes. *J. Neurosci.* **2015**, *35*, 10460–10473. [CrossRef]

11. Zhang, C.; Tabatabaei, M.; Bélanger, S.; Girouard, H.; Moeini, M.; Lu, X.; Lesage, F. Astrocytic endfoot Ca2+correlates with parenchymal vessel responses during 4-AP induced epilepsy: An in vivo two-photon lifetime microscopy study. *J. Cereb. Blood Flow Metab.* **2017**, *39*, 260–271. [CrossRef]

12. Chuquet, J.; Hollender, L.; Nimchinsky, E.A. High-Resolution In Vivo Imaging of the Neurovascular Unit during Spreading Depression. *J. Neurosci.* **2007**, *27*, 4036–4044. [CrossRef]

13. Rosenegger, D.G.; Tran, C.H.T.; Wamsteeker Cusulin, J.I.; Gordon, G.R. Tonic Local Brain Blood Flow Control by Astrocytes Independent of Phasic Neurovascular Coupling. *J. Neurosci.* **2015**, *35*, 13463–13474. [CrossRef] [PubMed]

14. Kur, J.; Newman, E.A. Purinergic control of vascular tone in the retina. *J. Physiol.* **2014**, *592*, 491–504. [CrossRef] [PubMed]

15. Mehina, E.M.F.; Murphy-Royal, C.; Gordon, G.R. Steady-state free Ca2+ in astrocytes is decreased by experience and impacts arteriole tone. *J. Neurosci.* **2017**, *37*, 0239-17. [CrossRef] [PubMed]

16. Rosenegger, D.G.; Tran, C.H.; LeDue, J.; Zhou, N.; Gordon, G.R. A high performance, cost-effective, open-source microscope for scanning two-photon microscopy that is modular and readily adaptable. *PLoS ONE* **2014**, *9*, e110475. [CrossRef] [PubMed]

17. Patton, C. *Webmaxc Standard, MaxChelator*; Stanford University: Stanford, CA, USA, 2009.

18. Henneberger, C.; Papouin, T.; Oliet, S.H.R.; Rusakov, D.A. Long-term potentiation depends on release of d-serine from astrocytes. *Nature* **2010**, *463*, 232–236. [CrossRef]

19. Parpura, V.; Haydon, P.G. Physiological astrocytic calcium levels stimulate glutamate release to modulate adjacent neurons. *Proc. Natl. Acad. Sci. USA* **2000**, *97*, 8629–8634. [CrossRef]

20. Kuchibhotla, K.V.; Lattarulo, C.R.; Hyman, B.T.; Brian, J.; Kuchibhotla, K.V.; Lattarulo, C.R.; Hyman, B.T.; Bacskai, B. Synchronous Hyperactivity and Intercellular Calcium Waves in Astrocytes in Alzheimer Mice. *Science* **2009**, *323*, 1211–1215. [CrossRef]

21. Zheng, K.; Bard, L.; Reynolds, J.P.; King, C.; Jensen, T.P.; Gourine, A.V.; Rusakov, D.A. Time-Resolved Imaging Reveals Heterogeneous Landscapes of Nanomolar Ca2+ in Neurons and Astroglia. *Neuron* **2015**, *88*, 277–288. [CrossRef]

22. Fordsmann, J.C.; Ko, R.W.Y.; Choi, H.B.; Thomsen, K.; Witgen, B.M.; Mathiesen, C.; Lønstrup, M.; Piilgaard, H.; MacVicar, B.A.; Lauritzen, M. Increased 20-HETE synthesis explains reduced cerebral blood flow but not impaired neurovascular coupling after cortical spreading depression in rat cerebral cortex. *J. Neurosci.* **2013**, *33*, 2562–2570. [CrossRef] [PubMed]

23. Pappas, A.C.; Koide, M.; Wellman, G.C. Purinergic signaling triggers endfoot high-amplitude Ca $^{2+}$ signals and causes inversion of neurovascular coupling after subarachnoid hemorrhage. *J. Cereb. Blood Flow Metab.* **2016**, *36*, 1901–1912. [CrossRef] [PubMed]

24. Zhu, S.; Han, G.; White, R.E. PGE2 action in human coronary artery smooth muscle: Role of potassium channels and signaling cross-talk. *J. Vasc. Res.* **2002**, *39*, 477–488. [CrossRef] [PubMed]

25. Takano, T.; Tian, G.-F.; Peng, W.; Lou, N.; Libionka, W.; Han, X.; Nedergaard, M. Astrocyte-mediated control of cerebral blood flow. *Nat. Neurosci.* **2006**, *9*, 260–267. [CrossRef]

26. Gebremedhin, D.; Lange, A.R.; Narayanan, J.; Aebly, M.R.; Jacobs, E.R.; Harder, D.R. Cat cerebral arterial smooth muscle cells express cytochrome P450 4A2 enzyme and produce the vasoconstrictor 20-HETE which enhances L-type Ca2+ current. *J. Physiol.* **1998**, *507*, 771–781. [CrossRef]

27. Tanaka, K.; Shibuya, I.; Kabashima, N.; Ueta, Y.; Yamashita, H. Inhibition of voltage-dependent calcium channels by prostaglandin E2 in rat melanotrophs. *Endocrinology* **1998**, *139*, 4801–4810. [CrossRef]

28. Sun, W.; McConnell, E.; Pare, J.-F.; Xu, Q.; Chen, M.; Peng, W.; Lovatt, D.; Han, X.; Smith, Y.; Nedergaard, M. Glutamate-Dependent Neuroglial Calcium Signaling Differs Between Young and Adult Brain. *Science* **2013**, *339*, 197–200. [CrossRef]

29. Bonder, D.E.; McCarthy, K.D. Astrocytic Gq-GPCR-Linked IP3R-Dependent Ca2+ Signaling Does Not Mediate Neurovascular Coupling in Mouse Visual Cortex In Vivo. *J. Neurosci.* **2014**, *34*, 13139–13150. [CrossRef]

30. Bazargani, N.; Attwell, D. Astrocyte calcium signaling: The third wave. *Nat. Neurosci.* **2016**, *19*, 182–189. [CrossRef]

31. Nizar, K.; Uhlirova, H.; Tian, P.; Saisan, P.A.; Cheng, Q.; Reznichenko, L.; Weldy, K.L.; Steed, T.C.; Sridhar, V.B.; MacDonald, C.L.; et al. In vivo Stimulus-Induced Vasodilation Occurs without IP3 Receptor Activation and May Precede Astrocytic Calcium Increase. *J. Neurosci.* **2013**, *33*, 8411–8422. [CrossRef]

32. Schummers, J.; Yu, H.; Sur, M. Tuned responses of astrocytes and their influence on hemodynamic signals in the visual cortex. *Science* **2008**, *320*, 1638–1643. [CrossRef]

33. Schulz, K.; Sydekum, E.; Krueppel, R.; Engelbrecht, C.J.; Schlegel, F.; Schröter, A.; Rudin, M.; Helmchen, F. Simultaneous BOLD fMRI and fiber-optic calcium recording in rat neocortex. *Nat. Methods* **2012**, *9*, 597–602. [CrossRef]

34. Winship, I.R.; Plaa, N.; Murphy, T.H. Rapid Astrocyte Calcium Signals Correlate with Neuronal Activity and Onset of the Hemodynamic Response In Vivo. *J. Neurosci.* **2007**, *27*, 6268–6272. [CrossRef]

35. Lind, B.; Brazhe, A.R.; Jessen, S.; Tan, F.C.C.; Lauritzen, M.J. Rapid stimulus-evoked astrocyte Ca 2+ elevations and hemodynamic responses in mouse somatosensory cortex in vivo. *Proc. Natl. Acad. Sci. USA* **2013**, *110*, E4678–E4687. [CrossRef]

36. Lecrux, C.; Toussay, X.; Kocharyan, A.; Fernandes, P.; Neupane, S.; Le, M.; Plaisier, F.; Shmuel, A.; Cauli, B.; Hamel, E.; et al. Pyramidal Neurons Are " Neurogenic Hubs " in the Neurovascular Coupling Response to Whisker Stimulation. *J. Neurosci.* **2011**, *31*, 9836–9847. [CrossRef] [PubMed]

37. Mishra, A.; Reynolds, J.P.; Chen, Y.; Gourine, A.V.; Rusakov, D.A.; Attwell, D. Astrocytes mediate neurovascular signaling to capillary pericytes but not to arterioles. *Nat. Neurosci.* **2016**, *19*, 1619–1627. [CrossRef]

38. Howarth, C.; Sutherland, B.A.; Choi, H.B.; Martin, C.; Lind, B.L.; Khennouf, L.; LeDue, J.M.; Pakan, J.M.P.; Ko, R.W.Y.; Ellis-Davies, G.; et al. A Critical Role for Astrocytes in Hypercapnic Vasodilation in Brain. *J. Neurosci.* **2017**, *37*, 2403–2414. [CrossRef] [PubMed]

39. Howarth, C. The contribution of astrocytes to the regulation of cerebral blood flow. *Front. Neurosci.* **2014**, *8*, 1–9. [CrossRef] [PubMed]

40. Mishra, A.; O'Farrell, F.M.; Reynell, C.; Hamilton, N.B.; Hall, C.N.; Attwell, D. Imaging pericytes and capillary diameter in brain slices and isolated retinae. *Nat. Protoc.* **2014**, *9*, 323–336. [CrossRef] [PubMed]

41. Niwa, K.; Haensel, C.; Ross, M.E.; Iadecola, C. Cyclooxygenase-1 participates in selected vasodilator responses of the cerebral circulation. *Circ. Res.* **2001**, *88*, 600–608. [CrossRef]

42. Lacroix, A.; Toussay, X.; Anenberg, E.; Lecrux, C.; Ferreiro, N.; Burgess, S.A.; Hillman, E.M.C.; Tegeder, I.; Murphy, T.H.; Hamel, E.; et al. COX-2-Derived Prostaglandin E2 Produced by Pyramidal Neurons Contributes to Neurovascular Coupling in the Rodent Cerebral Cortex. *J. Neurosci.* **2015**, *35*, 11791–11810. [CrossRef] [PubMed]

43. Peters, O.; Schipke, C.G.; Hashimoto, Y.; Kettenmann, H. Different Mechanisms Promote Astrocyte Ca2+ Waves and Spreading Depression in the Mouse Neocortex. *J. Neurosci.* **2003**, *23*, 9888–9896. [CrossRef] [PubMed]

44. Seidel, J.L.; Escartin, C.; Ayata, C.; Bonvento, G.; Shuttleworth, C.W. Multifaceted roles for astrocytes in spreading depolarization. *Glia* **2016**, *64*, 5–20. [CrossRef] [PubMed]